

Investigation of unsupervised and supervised hyperspectral anomaly detection

Mazharul Hossain^a, Aaron Robinson^b, Lan Wang^a, and Chrysanthé Preza^b

^aComputer Science Department

^bElectrical and Computer Engineering Department
The University of Memphis, Memphis, TN, USA

ABSTRACT

Hyperspectral sensing is a valuable tool for detecting anomalies and distinguishing between materials in a scene. Hyperspectral anomaly detection (HS-AD) helps characterize the captured scenes and separates them into anomaly and background classes. It is vital in agriculture, environment, and military applications such as RSTA (reconnaissance, surveillance, and target acquisition) missions. We previously designed an equal voting ensemble of hyperspectral unmixing and three unsupervised HS-AD algorithms. We later utilized a supervised classifier to determine the weights of a voting ensemble, creating a hybrid of heterogeneous unsupervised HS-AD algorithms with a supervised classifier in a model stacking, which improved detection accuracy. However, supervised classification methods usually fail to detect novel or unknown patterns that substantially deviate from those seen previously. In this work, we evaluate our technique and other supervised and unsupervised methods using general hyperspectral data to provide new insights.

Keywords: hyperspectral imaging, near-infrared NIR, remote sensing, unmanned aerial vehicles UAV, anomaly detection, machine learning, stacking ensemble learning

1. INTRODUCTION

Hyperspectral remote sensing is a technique that combines spectroscopy and imaging to collect spatial and spectral information and process information from across the electromagnetic spectrum. Hyperspectral imaging (HSI) aims to obtain the spectral information from a scene, and advancement of HSI technologies¹ combined with machine learning (ML) recognition techniques² promises improved scene characterization in numerous applications, such as the detection of anomalies in a large background, find objects, or identify materials. **Hyperspectral anomaly detection (HS-AD)**³ helps characterize the captured scenes and separates them into anomaly and background classes. Supervised anomaly detection solves this problem using data labeled with ground truth, whereas unsupervised anomaly detection does not.

Universality or generalization suggests that if a method achieves promising results on known datasets, it will perform similarly well for new or unseen data and provide consistent predictions. Usually, unsupervised HS-AD methods promise generalization as they should work well enough on unknown data. We previously introduced a new approach^{4,5} to the HS-AD problem using a supervised classifier as a meta-model in a stacking⁵ ensemble, which improved detection accuracy. However, our previous method does not generalize well when trained on one dataset and tested on other unfamiliar datasets. Unlike supervised ML models, unsupervised HS-AD methods should work well enough on unknown data. Unfortunately, our evaluation found unsupervised HS-AD methods are not consistently generalizing, and their performance varies from dataset to dataset.

This treatment presents our unsupervised stacking-ensemble anomaly detection approach to solve the generalization problem. We have utilized the Greedy search⁵ approach to find suitable HS-AD methods for the base model and unsupervised Gaussian mixture model as the meta-model. We believe this approach holds significant potential for improving generalized anomaly detection accuracy. We have considered twenty-two scenes from four public and one private benchmarking datasets (thirteen scenes from the ABU (airport, beach, and urban) dataset, five from the Arizona dataset, two from the San Diego airport dataset, and one from each of the HY-DICE urban and Salinas datasets). We used 2-fold cross-validation five times to show our methods' statistical

Further author information: (Send correspondence to Mazharul Hossain); E-mail: mhossain9@memphis.edu

significance, where it achieved an average ROC-AUC score of 0.918 with a standard deviation of 0.131, which is at least seven % better than other individual methods. This article also investigates other supervised and unsupervised methods using these datasets. We compare the ROC-AUC scores to provide new insights and recommendations on the performance. Continuous improvement and innovation in this research area are crucial in further enhancing the general accuracy of hyperspectral anomaly detection and advancing the hyperspectral sensing field.

2. BACKGROUND

Hyperspectral imagers are expensive, and only a few standard HS datasets are available.⁶ As a result, most researchers are exploring unsupervised HS-AD algorithms⁷ that do not require annotated data, such as those based on statistical methods.³

2.1 Individual Hyperspectral Anomaly Detection Algorithms

The researchers and reviewers categorize hyperspectral anomaly detection (HS-AD) methods based on the design criteria to separate the background and anomalies and also based on the primary function model.^{3,7,8} The Reed–Xiaoli (RX),^{9,10} MD–RX, and Windowed RX (WIN-RX) are some examples of Statistics-based HS-AD techniques. Subspace-RX (SSRX),¹¹ Complementary Subspace Detector (CSD),¹² Local Summation Anomaly Detection (LSAD),¹³ Local Summation Unsupervised Nearest Regularized Subspace with an Outlier Removal Anomaly Detector (LSUNRSORAD)¹⁴ are some examples of subspace-based techniques. Kernel–RX Algorithm (KRX),^{15,16} Gaussian Mixture RX (GM-RX)¹⁷ are some examples of kernel-based techniques. Cluster-based anomaly detector (CBAD),¹⁸ fuzzy c-means clustering-based anomaly detector (FCBAD)¹⁹ are some examples of clustering distance-based techniques. Attribute and Edge-Preserving Filters (AED)²⁰ is an example of spatial-spectral filtering-based techniques. Isolation forest (iForest)²¹ is an example of Machine learning-based techniques. Kernel iForest (KIFD)²² combines both kernel-based and ML-based techniques. We found that each method’s performance depends upon specific background characteristic constraints and is effective only in some scenarios. Thus, we investigated to find a combination of methods to overcome this limitation.

2.2 Ensemble Hyperspectral Anomaly Detection Algorithms

Yang et al.²³ proposed an Ensemble and Random RX with Multiple Features (ERRX MF) anomaly detector using three features, Gabor, Extended Morphological Profile (EMP), and Extended Multiattribute Profile (EMAP), along with the original hyperspectral image. Wang et al.²⁴ proposed a sub-feature ensemble called SED. They randomly sub-sampled channels and used six heterogeneous base models in the ensemble. Finally, a prior-based tensor approximation algorithm (PTA)²⁵ used these sub-features for anomaly detection. Fatemifar et al.²⁶ proposed a stacking ensemble for face spoofing anomaly detection that consisted of 63 base classifiers and a Gaussian Mixture Model (GMM) as the meta-classifier for the second stage. Younis et al.⁴ proposed an equal-weight voting method called Hyperspectral Unmixing-Based Voting Ensemble Anomaly Detector (HUE-AD) that combines four detectors (Abundance, AED, KIFD, and LSUNRSORAD) to identify anomalies. Hossain et al.⁵ proposed a stacking ensemble called Greedy Ensemble Hyperspectral Anomaly Detector (GE-AD) that uses a greedy search algorithm to find four suitable base detectors and utilizes a supervised machine learning model to combine those four base detectors to identify anomalies. Figure 1 shows the overall flowchart of the GE-AD algorithm. The greedy search algorithm uses 2-fold cross-validation to evaluate performance metrics and greedily searches for base methods to maximize the performance score, which reduces the search space compared to a grid search approach. This method produces a much higher F1-macro score and similar ROC-AUC score than the input methods.

3. METHODOLOGY

We optimized the HUE-AD and GE-AD in this treatment to improve their generalizability. We also investigated some unsupervised ML models as meta-models. Unlike the F1 score, we found that improving the ROC-AUC score in one dataset translates to a better ROC-AUC score in another. Thus, we tried to maximize the ROC-AUC score using the greedy search. In this section, we discussed our methodology in detail.

3.1 Hyperspectral Unmixing-Based Voting Ensemble Anomaly Detector (HUE-AD)

Our empirical tests found that HUE-AD⁴’s three base anomaly detectors can operate adequately in a trio even when the particular spectra of interest or their abundances are unknown. Thus, under our new modification, we

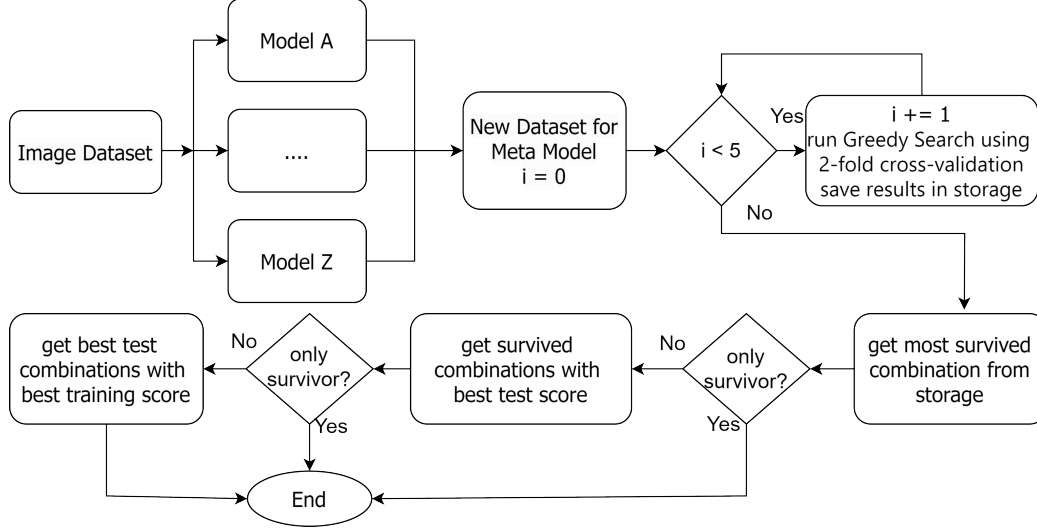


Figure 1. Overall flowchart of GE-AD⁵ to find the best AD methods for ensemble fusion.

skip the abundance and determine a pixel as anomalous if at least two base methods vote a pixel as anomalous. Although not as good as the original HUE-AD, the performance was acceptable and still has a higher F1-macro score than the input methods. As it has a lower ROC-AUC score, we modified it further and used an average ensemble using the input results without binarizing to find the anomaly score. We are calling it the baseline in our investigation.

3.2 Greedy Ensemble Hyperspectral Anomaly Detector (GE-AD)

GE-AD⁵ is a stacking ensemble that uses a supervised machine learning model as a meta-model that combines four detectors to identify anomalies. GE-AD utilizes a greedy search algorithm to find those four suitable detectors to maximize the scoring function. However, the trained model does not generalize and suffers when applied to an unfamiliar new scene. Thus, along with four base methods, we used thirty normalized random channels as input to the supervised meta-classifier. We expect the classifier to learn about the underlying dataset and generalize better. Our results show better ROC-AUC scores than before. We are calling this modified version the mGE-AD in our investigation.

3.3 Proposed Unsupervised Ensemble Approach (UGE-AD)

We have utilized the same greedy search⁵ approach to find suitable HS-AD methods as the base model. We considered the Reed–Xiaoli (RX)^{9,10} detector, Attribute and Edge-Preserving Filters (AED),²⁰ Cluster-based anomaly detector (CBAD),¹⁸ Complementary Subspace Detector (CSD),¹² Fuzzy clustering-based anomaly detector (FCBAD),¹⁹ Gaussian mixture RX (GM-RX)¹⁷ anomaly detector, Kernel iForest (KIFD)²² anomaly detector, Local Summation Unsupervised Nearest Regularized Subspace with an Outlier Removal Anomaly Detector (LSUNRSORAD),¹⁴ Median RX (MD-RX) anomaly detector, Subspace-RX (SSRX),¹¹ Windowed RX (WIN-RX).

The RX^{9,10} detector has a simple statistical principle, low computational complexity, and relatively good performance. It characterizes the background using the HSI’s mean and covariance and calculates the Mahalanobis distance²⁷ between the background and pixel under test. As the mean is very susceptible to noise, MD-RX uses the median instead of the mean as statistical information to improve RX. Meanwhile, WIN-RX uses a sliding window to calculate local mean and covariance and determine anomalies. GM-RX¹⁷ uses the Gaussian Mixture Model (GMM) to characterize the complex scene to improve the detection of the RX algorithm. Schaum et al.¹¹ in SSRX deleted several high-variance Principal Components (PC) dimensions as background clutters found in principal component analysis (PCA) to improve the RX performance. They later designed CSD¹² where the highest variance PCs define the background subspace and the others (the complementary subspace) as the target subspace. Carlotto, Mark J.¹⁸ proposed that the image background can be divided into clusters in the CBAD algorithm. FCBAD¹⁹ improved the CBAD using fuzzy c-means clustering instead of k-means clustering.

Kang et al.²⁰ assumed that anomalies tend to be smaller and possess unique reflectance signatures and that the pixels belonging to the same class would have a high correlation in the spatial domain, and based on this principle, they proposed AED. Tan et al.¹⁴ proposed LSUNRSORAD to decrease the computational complexity of LSAD.¹³ Li et al.²² utilized the kernel space of PCA and the isolation forest (iForest)²¹ to isolate anomalies in their proposed KIFD²² algorithm.

We considered a similar idea to Wang et al.²⁴ and Fatemifar et al.²⁶ and investigated multiple unsupervised methods as meta-model. We used the Gaussian mixture model for the meta-model. We also investigated Forest; however, it did not perform well.

We have considered the proposed methodology of Yang et al.²³ Instead of directly passing through the HSI data, we utilized PCA to find ten PCs as a passthrough to the meta-model to improve the ROC-AUC score.

3.4 Datasets

We assessed the AD algorithms' effectiveness using twenty-two scenes from six public and one private benchmarking datasets. These scenes are from the Airport–Beach–Urban (ABU) dataset,^{20,28} the San Diego dataset,^{29,30} the Salinas dataset,³¹ the Hydice Urban dataset,^{32,33} and the Arizona dataset.³⁴

The ABU airport and beach datasets have four scenes, whereas the ABU urban and the Arizona datasets have five. The San Diego airport dataset has two scenes. Both the HYDICE urban and the Salinas datasets have one scene each. Salinas dataset contains a farming field, whereas HYDICE urban has some urban development within vast vegetation. The ABU urban contains urban scenes. Arizona dataset contains a sandy desert scene with sparse vegetation and no urban development. The ABU beach contains scenes with water, which is challenging because of it. The ABU airport and the San Diego airport contain similar scenes from airports.

4. RESULTS

Our research aims to assist the decision-making processes of the human in the loop. Therefore, our performance goal was to identify all anomalies accurately and minimize the misclassification of positive instances as negative because humans can overlook the misclassification of a negative case as positive. To evaluate the HS-AD algorithms, we utilized the traditional classification evaluation metric known as the area under the receiver operating characteristic (ROC) curve (ROC-AUC) score,^{35–37} which is suitable for assessing this scenario.

For our first evaluation, we used only one dataset in the greedy search to identify suitable base methods for UGE-AD, aiming to maximize the ROC-AUC score. The results are shown in Table 1. Figure 2 helps us understand the results better than the table format. The results show that the greedy search may fail to find the optimal base methods for smaller datasets, and the results generalize more effectively for larger datasets. Table 1 shows that the performances are correlated to input base methods instead of the scene similarity. As we can see, GM-RX helps get a suitable performance score for the San Diego airport dataset. Another issue was that greedy search could find a better score for the Arizona and Salinas datasets. However, only GM-RX was sufficient for the Arizona dataset, as shown in Table 1.

For our second evaluation, from the twenty-two scenes from six public and one private benchmarking datasets, the GE-AD algorithm randomly selected datasets to ensure we have at least 50% image scenes are assigned to the greedy search. Over five runs with 2-fold cross-validation, greedy search tried to maximize the ROC-AUC score and selected AED, FCBAD, GM-RX, and KIFD as base methods for our unsupervised GE-AD. In our unsupervised GE-AD, we used these four base methods and ten PCs as inputs to the GMM meta-model. UGE-AD achieved an average of 0.943 ROC-AUC scores with a standard deviation (STD) of 0.088, which is lower than other input methods, as shown in Table 2 over seven datasets. The greedy search selected GM-RX, KIFD, LSUNRSORAD, and MD-RX as base methods for our supervised mGE-AD. We used these four base methods and thirty random channels from the HSI as inputs to the random forest (RF) meta-classifier. mGE-AD achieved an average of 0.882 ROC-AUC score with an STD of 0.170. Our baseline HUE-AD did not need any training. It is an averaging ensemble of AED, KIFD, and LSUNRSORAD achieved an average of 0.902 ROC-AUC score with an STD of 0.201. Table 3 shows F1-macro scores of these three ensembles. mGE-AD achieved the best average F1-macro score of 0.593 with an STD of 0.070. Although UGE-AD had the lowest STD of 0.048, suggesting a stable solution compared to others, there is still room for improvement.

Table 1. Average ROC-AUC scores of our newly proposed Unsupervised ensemble UGE-AD over various datasets. The first column shows the dataset used in the greedy search to find suitable base methods, and the second column shows those base methods. Where the dataset names in rows and columns match, those cells show the training score after the greedy search.

		HYDICE	Salinas	San Diego	ABU airport	ABU beach	ABU urban	Arizona
HYDICE	WIN-RX	0.997	0.951	0.962	0.943	0.963	0.964	0.802
Salinas	LSUNRSORAD, RX	0.995	0.999	0.965	0.949	0.971	0.971	0.780
San Diego	GM-RX	0.997	0.997	0.964	0.934	0.961	0.962	0.847
ABU airport	AED, GM-RX, KIFD, LSUNRSORAD	0.995	1.000	0.971	0.962	0.985	0.966	0.712
ABU beach	KIFD, LSUNRSORAD, RX, WIN-RX	0.996	0.997	0.965	0.960	0.973	0.976	0.766
ABU urban	AED, KIFD, LSUNRSORAD, RX	0.996	1.000	0.970	0.962	0.985	0.971	0.706
Arizona	CBAD, FCBAD, GM-RX, KIFD	0.994	0.999	0.972	0.948	0.967	0.966	0.779

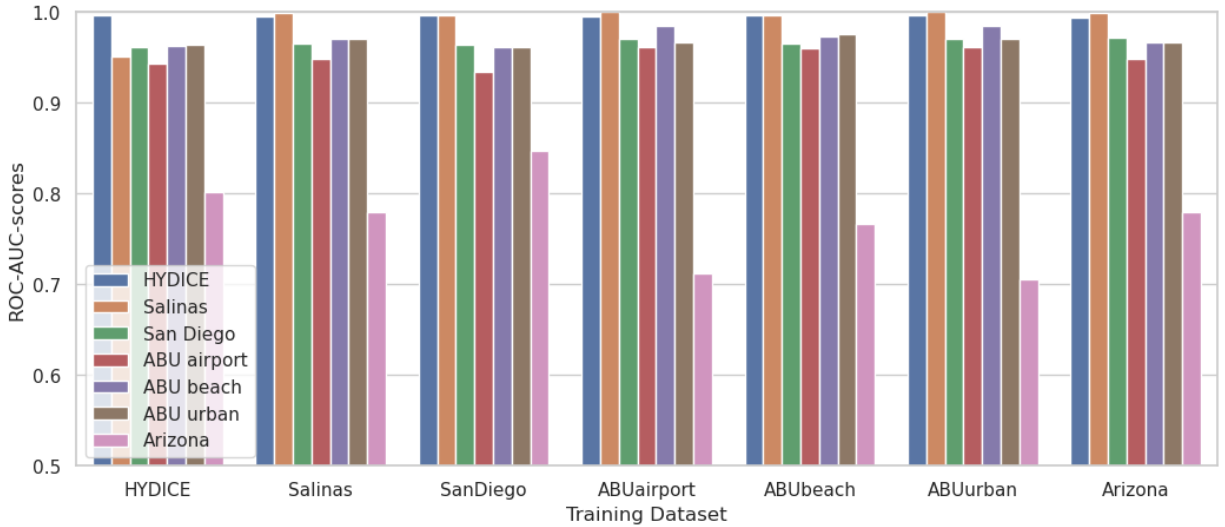


Figure 2. Average ROC-AUC scores of our UGE-AD over various datasets showing consistent performance against various training datasets. The X-axis shows the dataset used in the greedy search to find suitable base methods. The Y-axis shows the testing ROC AUC scores. Except where the dataset names in rows and columns match, those bars show the training score after the greedy search.

The results from San Diego airport, HYDICE urban, and Salinas datasets are in Table 4. UGE-AD has the highest average in the HYDICE urban dataset. However, LSUNRSORAD and our baseline HUE-AD achieved a perfect score in the Salinas dataset. The baseline HUE-AD scores are better than others for the first scene of the San Diego airport dataset, whereas AED performed best in the second scene. The individual results from the ABU airport dataset are shown in Table 5, where LSUNRSORAD in the first scene, AED performed best in the second and fourth scenes, and baseline HUE-AD in the third scene. The individual results from the ABU beach dataset are shown in Table 6, where AED performed best in the first scene, baseline HUE-AD in the second scene, and UGEE-AD in the fourth scene. However, most of the algorithms got perfect scores in the third scene. The individual results from the ABU urban dataset are shown in Table 7, where AED performed best in the first and third scenes, RX in the second scene, CSD and MD-RX along with RX in the fourth scene, and baseline HUE-AD in the fifth scene. Table 8 shows the Arizona dataset results, where GM-RX performed best in the fourth scene and UGE-AD in all four other scenes.

From our results, it is evident that AED gets better results most of the time. Along with KIFD and LSUNRSORAD, it performs better consistently. Our baseline HUE-AD showed more promising results than UGE-AD. However, UGE-AD showed its performance in the Arizona dataset, where all other HS-AD methods failed. It performed well as the meta-model had access to PCs as input, which helped avoid the pitfall when input base models failed.

Table 2. Average and standard deviation of ROC-AUC scores of various methods computed over the ABU, Arizona, HYDICE urban, Salinas, and San Diego datasets.

Methods	HYDICE urban	Salinas	San Diego	ABU airport	ABU beach	ABU urban	Arizona	Average score
CBAD	0.970	0.390	0.611	0.753	0.681	0.466	0.566	0.634±0.178
CSD	0.982	0.788	0.906	0.877	0.962	0.979	0.451	0.849±0.175
FCBAD	0.994	0.841	0.964	0.910	0.973	0.904	0.508	0.870±0.156
GM-RX	0.957	0.546	0.388	0.599	0.901	0.651	0.497	0.648±0.194
MD-RX	0.986	0.817	0.923	0.869	0.961	0.977	0.453	0.855±0.174
RX	0.985	0.807	0.915	0.886	0.962	0.979	0.451	0.855±0.175
SSRX	0.747	0.848	0.802	0.758	0.925	0.848	0.589	0.788±0.099
WIN-RX	0.749	0.798	0.705	0.807	0.934	0.857	0.541	0.770±0.116
AED	0.979	0.956	0.988	0.979	0.983	0.923	0.392	0.886±0.203
KIFD	0.830	0.995	0.991	0.964	0.948	0.962	0.652	0.906±0.116
LSUNRSORAD	0.994	1.000	0.945	0.964	0.989	0.973	0.353	0.888±0.219
baseline HUE-AD (AED, KIFD, LSUNRSORAD)	0.962	1.000	0.988	0.980	0.986	0.987	0.411	0.902±0.201
mGE-AD (GM-RX, KIFD, LSUNRSORAD, MD-RX), RF	0.927	0.997	0.939	0.907	0.965	0.970	0.472	0.882±0.170
UGE-AD (AED, FCBAD, GM-RX, KIFD), GMM	0.995	0.999	0.970	0.960	0.980	0.968	0.731	0.943±0.088

Table 3. Average and standard deviation of F1-macro scores of our ensemble methods computed over the ABU, Arizona, HYDICE urban, Salinas, and San Diego datasets.

Methods	HYDICE urban	Salinas	San Diego	ABU airport	ABU beach	ABU urban	Arizona	Average score
baseline HUE-AD	0.519	0.512	0.619	0.629	0.564	0.663	0.541	0.578 ± 0.055
mGE-AD	0.525	0.729	0.560	0.584	0.628	0.624	0.503	0.593 ± 0.070
UGE-AD	0.500	0.480	0.559	0.566	0.514	0.605	0.613	0.548 ± 0.048

5. CONCLUSION

Our research showed that various approaches do not always give generalized results, as demonstrated by the higher standard deviation (STD). Our new stack ensemble method with an unsupervised GMM meta-model shows generalization and more reliable results with less variation through better average and lower STD ROC AUC score, which is a positive development. We plan to explore it further in future research. This unsupervised method provides a better ROC AUC score. In contrast, the stack ensemble method with a supervised Random Forest meta-model ensures a better F1-macro score. We plan to design an HS-AD method that enhances ROC AUC and F1 scores. We plan to investigate other supervised and unsupervised methods as meta-models and evaluate the impact of various thresholding methods and scoring functions on performance.

APPENDIX A. QUANTITATIVE EVALUATION

Detailed quantitative results will help us understand the performance of this anomaly detection model. Tables 4, 5, 6, 7, and 8 present prediction metrics for individual methods and our ensemble methods for each HS image across all datasets.

Table 4. Comparison of ROC-AUC scores between various methods using the HYDICE urban, Salinas, and San Diego datasets

Methods	HYDICE urban	Salinas	San Diego-01	San Diego-02
CBAD	0.970	0.390	0.674	0.547
CSD	0.982	0.788	0.941	0.871
FCBAD	0.994	0.841	0.969	0.958
GM-RX	0.957	0.546	0.557	0.219
MD-RX	0.986	0.817	0.945	0.900
RX	0.985	0.807	0.940	0.889
SSRX	0.747	0.848	0.768	0.836
WIN-RX	0.749	0.798	0.656	0.753
AED	0.979	0.956	0.985	0.991
KIFD	0.830	0.995	0.992	0.989
LSUNRSORAD	0.994	1.000	0.980	0.910
baseline HUE-AD	0.962	1.000	0.993	0.982
mGE-AD	0.927	0.997	0.916	0.962
UGE-AD	0.995	0.999	0.976	0.964

ACKNOWLEDGMENTS

This research was sponsored by the Army Research Laboratory and was accomplished under Cooperative Agreement Number W911NF-21-2-0294 with Eddie L. Jacobs as PI. The views and conclusions contained in this

Table 5. Comparison of ROC-AUC scores between various methods using the ABU airport dataset

Methods	ABU-airport-1	ABU-airport-2	ABU-airport-3	ABU-airport-4
CBAD	0.858	0.633	0.633	0.886
CSD	0.824	0.826	0.922	0.934
FCBAD	0.877	0.880	0.897	0.986
GM-RX	0.674	0.590	0.680	0.453
MD-RX	0.813	0.841	0.925	0.896
RX	0.822	0.840	0.929	0.953
SSRX	0.639	0.857	0.892	0.644
WIN-RX	0.774	0.797	0.949	0.708
AED	0.969	0.994	0.957	0.995
KIFD	0.940	0.979	0.961	0.975
LSUNRSORAD	0.972	0.959	0.966	0.959
baseline HUE-AD	0.970	0.989	0.973	0.988
mGE-AD	0.859	0.916	0.920	0.931
UGE-AD	0.933	0.971	0.948	0.986

Table 6. Comparison of ROC-AUC scores between various methods using the ABU beach dataset

Methods	ABU-beach-1	ABU-beach-2	ABU-beach-3	ABU-beach-4
CBAD	0.571	0.603	0.664	0.885
CSD	0.982	0.911	1.000	0.956
FCBAD	0.987	0.955	1.000	0.948
GM-RX	0.986	0.701	1.000	0.916
MD-RX	0.980	0.910	1.000	0.955
RX	0.981	0.911	1.000	0.954
SSRX	0.980	0.906	0.982	0.831
WIN-RX	0.957	0.962	1.000	0.815
AED	0.997	0.955	1.000	0.979
KIFD	0.990	0.989	0.998	0.813
LSUNRSORAD	0.994	0.986	1.000	0.975
baseline HUE-AD	0.992	0.992	1.000	0.958
mGE-AD	0.962	0.980	0.981	0.935
UGE-AD	0.995	0.946	1.000	0.980

Table 7. Comparison of ROC-AUC scores between various methods using the ABU urban dataset

Methods	ABU-urban-1	ABU-urban-2	ABU-urban-3	ABU-urban-4	ABU-urban-5
CBAD	0.391	0.155	0.613	0.598	0.573
CSD	0.991	0.994	0.950	0.989	0.969
FCBAD	0.992	0.851	0.941	0.847	0.891
GM-RX	0.760	0.549	0.778	0.765	0.402
MD-RX	0.991	0.994	0.939	0.989	0.970
RX	0.991	0.995	0.951	0.989	0.969
SSRX	0.928	0.989	0.748	0.786	0.791
WIN-RX	0.927	0.909	0.783	0.787	0.881
AED	0.998	0.796	0.998	0.840	0.984
KIFD	0.938	0.917	0.992	0.978	0.984
LSUNRSORAD	0.996	0.972	0.988	0.928	0.983
baseline HUE-AD	0.993	0.972	0.996	0.985	0.990
mGE-AD	0.980	0.935	0.985	0.968	0.981
UGE-AD	0.977	0.976	0.962	0.973	0.952

Table 8. Comparison of ROC-AUC scores between various methods using the Arizona dataset

Methods	Arizona 1	Arizona 2	Arizona 3	Arizona 4	Arizona 5
CBAD	0.510	0.374	0.556	0.742	0.648
CSD	0.335	0.410	0.601	0.264	0.645
FCBAD	0.367	0.432	0.662	0.350	0.727
GM-RX	0.576	0.271	0.457	0.760	0.423
MD-RX	0.334	0.410	0.602	0.271	0.648
RX	0.334	0.410	0.602	0.262	0.647
SSRX	0.564	0.578	0.661	0.458	0.682
WIN-RX	0.534	0.507	0.629	0.437	0.596
AED	0.329	0.326	0.492	0.307	0.504
KIFD	0.580	0.567	0.671	0.663	0.780
LSUNRSORAD	0.208	0.369	0.501	0.187	0.499
baseline HUE-AD	0.248	0.465	0.551	0.216	0.573
mGE-AD	0.427	0.290	0.622	0.382	0.639
UGE-AD	0.671	0.695	0.925	0.458	0.905

document are those of the authors and should not be interpreted as representing the official policies, either expressed or implied, of the Army Research Office or the US Government. The US Government is authorized to reproduce and distribute reprints for Government purposes notwithstanding any copyright notation herein.

This material is based upon work supported by the National Science Foundation while Lan Wang was serving at the National Science Foundation. Any opinion, findings, and conclusions or recommendations expressed in this material are those of the author(s) and do not necessarily reflect the views of the National Science Foundation.

REFERENCES

- [1] Khan, M. J., Khan, H. S., Yousaf, A., Khurshid, K., and Abbas, A., “Modern trends in hyperspectral image analysis: A review,” *IEEE Access* **6**, 14118–14129 (2018).
- [2] Paoletti, M., Haut, J., Plaza, J., and Plaza, A., “Deep learning classifiers for hyperspectral imaging: A review,” *ISPRS Journal of Photogrammetry and Remote Sensing* **158**, 279–317 (2019).
- [3] Su, H., Wu, Z., Zhang, H., and Du, Q., “Hyperspectral anomaly detection: A survey,” *IEEE Geoscience and Remote Sensing Magazine* **10**(1), 64–90 (2021).
- [4] Younis, M. S., Hossain, M., Robinson, A. L., Wang, L., and Preza, C., “Hyperspectral unmixing-based anomaly detection,” in *[Computational Imaging VII]*, **12523**, 1252302, SPIE (2023).
- [5] Hossain, M., Younis, M., Robinson, A., Wang, L., and Preza, C., “Greedy ensemble hyperspectral anomaly detection,” *Journal of Imaging* **10**(6), 131 (2024).
- [6] Hu, X., Xie, C., Fan, Z., Duan, Q., Zhang, D., Jiang, L., Wei, X., Hong, D., Li, G., Zeng, X., et al., “Hyperspectral anomaly detection using deep learning: A review,” *Remote Sensing* **14**(9), 1973 (2022).
- [7] Xu, Y., Zhang, L., Du, B., and Zhang, L., “Hyperspectral anomaly detection based on machine learning: An overview,” *IEEE Journal of Selected Topics in Applied Earth Observations and Remote Sensing* **15**, 3351–3364 (2022).
- [8] Raza Shah, N., Maud, A. R. M., Bhatti, F. A., Ali, M. K., Khurshid, K., Maqsood, M., and Amin, M., “Hyperspectral anomaly detection: a performance comparison of existing techniques,” *International Journal of Digital Earth* **15**(1), 2078–2125 (2022).
- [9] Reed, I. S. and Yu, X., “Adaptive multiple-band cfar detection of an optical pattern with unknown spectral distribution,” *IEEE Transactions on acoustics, speech, and signal processing* **38**(10), 1760–1770 (1990).
- [10] Chang, C.-I. and Chiang, S.-S., “Anomaly detection and classification for hyperspectral imagery,” *IEEE Transactions on geoscience and remote sensing* **40**(6), 1314–1325 (2002).
- [11] Schaum, A. P. and Stocker, A. D., “Joint hyperspectral subspace detection derived from a bayesian likelihood ratio test,” in *[Algorithms and Technologies for Multispectral, Hyperspectral, and Ultraspectral Imagery VIII]*, **4725**, 225–233, SPIE (2002).
- [12] Schaum, A., “Hyperspectral anomaly detection beyond rx,” in *[Algorithms and Technologies for Multispectral, Hyperspectral, and Ultraspectral Imagery XIII]*, **6565**, 13–25, SPIE (2007).
- [13] Du, B., Zhao, R., Zhang, L., and Zhang, L., “A spectral-spatial based local summation anomaly detection method for hyperspectral images,” *Signal Processing* **124**, 115–131 (2016).
- [14] Tan, K., Hou, Z., Wu, F., Du, Q., and Chen, Y., “Anomaly detection for hyperspectral imagery based on the regularized subspace method and collaborative representation,” *Remote sensing* **11**(11), 1318 (2019).
- [15] Kwon, H. and Nasrabadi, N. M., “Kernel rx-algorithm: A nonlinear anomaly detector for hyperspectral imagery,” *IEEE Transactions on Geoscience and Remote Sensing* **43**(2), 388–397 (2005).
- [16] Hidalgo, J. A. P., Pérez-Suay, A., Nar, F., and Camps-Valls, G., “Efficient nonlinear rx anomaly detectors,” *IEEE Geoscience and Remote Sensing Letters* **18**(2), 231–235 (2020).
- [17] Acito, N., Diani, M., and Corsini, G., “Gaussian mixture model based approach to anomaly detection in multi/hyperspectral images,” in *[Image and Signal Processing for Remote Sensing XI]*, **5982**, 209–217, SPIE (2005).
- [18] Carlotto, M. J., “A cluster-based approach for detecting man-made objects and changes in imagery,” *IEEE Transactions on Geoscience and Remote Sensing* **43**(2), 374–387 (2005).
- [19] Hytla, P. C., Hardie, R. C., Eismann, M. T., and Meola, J., “Anomaly detection in hyperspectral imagery: comparison of methods using diurnal and seasonal data,” *Journal of Applied Remote Sensing* **3**(1), 033546 (2009).
- [20] Kang, X., Zhang, X., Li, S., Li, K., Li, J., and Benediktsson, J. A., “Hyperspectral anomaly detection with attribute and edge-preserving filters,” *IEEE Transactions on Geoscience and Remote Sensing* **55**(10), 5600–5611 (2017).
- [21] Liu, F. T., Ting, K. M., and Zhou, Z.-H., “Isolation forest,” in *[2008 eighth ieee international conference on data mining]*, 413–422, IEEE (2008).

- [22] Li, S., Zhang, K., Duan, P., and Kang, X., “Hyperspectral anomaly detection with kernel isolation forest,” *IEEE Transactions on Geoscience and Remote Sensing* **58**(1), 319–329 (2019).
- [23] Yang, X., Huang, X., Zhu, M., Xu, S., and Liu, Y., “Ensemble and random rx with multiple features anomaly detector for hyperspectral image,” *IEEE Geoscience and Remote Sensing Letters* **19**, 1–5 (2022).
- [24] Wang, S., Feng, W., Quan, Y., Bao, W., Dauphin, G., Gao, L., Zhong, X., and Xing, M., “Subfeature ensemble-based hyperspectral anomaly detection algorithm,” *IEEE Journal of Selected Topics in Applied Earth Observations and Remote Sensing* **15**, 5943–5952 (2022).
- [25] Li, L., Li, W., Qu, Y., Zhao, C., Tao, R., and Du, Q., “Prior-based tensor approximation for anomaly detection in hyperspectral imagery,” *IEEE Transactions on Neural Networks and Learning Systems* **33**(3), 1037–1050 (2020).
- [26] Fatemifar, S., Awais, M., Akbari, A., and Kittler, J., “A stacking ensemble for anomaly based client-specific face spoofing detection,” in [2020 *IEEE International Conference on Image Processing (ICIP)*], 1371–1375, IEEE (2020).
- [27] Mahalanobis, P. C., “On the generalized distance in statistics,” *Sankhyā: The Indian Journal of Statistics, Series A (2008-)* **80**, S1–S7 (2018).
- [28] Kang, X., “Airport-Beach-Urban (ABU) Datasets.” <http://xudongkang.weebly.com/data-sets.html> (2017). Accessed: 2023-04-23.
- [29] Zhao, Y.-Q. and Yang, J., “Hyperspectral image denoising via sparse representation and low-rank constraint,” *IEEE Transactions on Geoscience and Remote Sensing* **53**(1), 296–308 (2014).
- [30] Zhu, L. and Wen, G., “Hyperspectral anomaly detection via background estimation and adaptive weighted sparse representation,” *Remote Sensing* **10**(2), 272 (2018).
- [31] M Graña, MA Veganzons, B. A., “Hyperspectral remote sensing scenes.” University of the Basque Country (2001). Accessed: 2024-01-13.
- [32] Li, W., Wu, G., and Du, Q., “Transferred deep learning for anomaly detection in hyperspectral imagery.” Git Hub (2019). Accessed: 2024-01-13.
- [33] Kalman, L. S. and Bassett III, E. M., “Classification and material identification in an urban environment using hydice hyperspectral data,” in [*Imaging Spectrometry III*], **3118**, 57–68, SPIE (1997).
- [34] Watson, T. P., McKenzie, K., Robinson, A., Renshaw, K., Driggers, R., Jacobs, E. L., and Conroy, J., “Evaluation of aerial real-time rx anomaly detection,” in [*Algorithms, Technologies, and Applications for Multispectral and Hyperspectral Imaging XXIX*], **12519**, 254–260, SPIE (2023).
- [35] Hanley, J. A. and McNeil, B. J., “The meaning and use of the area under a receiver operating characteristic (roc) curve,” *Radiology* **143**(1), 29–36 (1982).
- [36] Chang, C.-I., “Comprehensive analysis of receiver operating characteristic (roc) curves for hyperspectral anomaly detection,” *IEEE Transactions on Geoscience and Remote Sensing* **60**, 1–24 (2022).
- [37] rasharmaravindrasharma, r., “Auc-roc curve.” <https://www.geeksforgeeks.org/auc-roc-curve/> (January 2022). Accessed: 2024-01-13.